ACS OMEGA

http://pubs.acs.org/journal/acsodf

Article

Synthesis of Cu_2O Nanoparticles by Ellipse Curve Micromixer

Xin Wang, Zhanqiang Liu,* Yukui Cai, Qinghua Song, and Bing Wang

Cite This: *ACS Omega* 2023, 8, 29758−29769

Read Online

ACCESS | Metrics & More | Article Recommendations

ABSTRACT: Micromixers offer the advantage of rapid and homogeneous mixing compared with conventional macroscale reaction systems, and thus they show great potential for the synthesis of nanoparticles. An ellipse curve serpentine micromixer, which had been proposed in our prior works was employed to synthesize Cu_2O nanoparticles. Cu_2O are excellent photocatalysts that have been widely utilized in the degradation of organic dyes. Owing to the excellent mixing performance, the reduction of $Cu(OH)_2$ in micromixing synthesis was more sufficient than that in conventional stirring synthesis. The Cu_2O nanoparticles synthesized by micromixing had smaller size and narrower size distribution compared with those synthesized by stirring in a beaker. The smallest Cu_2O nanoparticles were obtained by micromixing with Re = 100 at T = 60 °C, while the most uniform Cu_2O nanoparticles were obtained at T = 80 °C owing to Ostwald ripening. Through the photocatalytic degradation experiments of Rhodamine B, the Cu_2O nanoparticles synthesized by micromixing were found to have better photocatalysis than those synthesized by stirring. The research results showed that the micromixing synthesis was a more suitable choice to produce Cu_2O nanoparticles with excellent photocatalysis. The ellipse curve micromixer with a simple structure and high mixing performance can be applied in the synthesis of various nanoparticles.

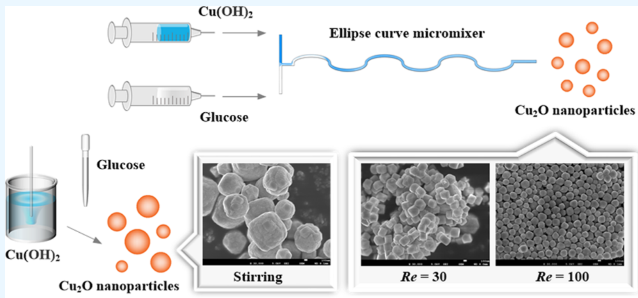

1. INTRODUCTION

Cu_2O nanoparticles have attracted great attention on account of their widespread application scenarios including antibacterials,[1] sensors,[2] catalysts,[3] colorants,[4] and batteries.[5] One of the most common uses of Cu_2O is the photocatalytic degradation of organic dyes.[6−8] Cu_2O is a p-type semiconductor that has a narrow band gap and a wide spectrum absorption range. Electron−hole pairs can be readily generated in Cu_2O under irradiation. The photogenerated electrons or holes would move to the surfaces of Cu_2O nanoparticles and undergo redox reactions with the electron acceptors or electron donors absorbed on nanoparticle surfaces to degrade the organic dyes.

The liquid phase reducing method was a convenient approach to produce Cu_2O nanoparticles due to the low equipment requirements, high operating flexibility, and low costs.[9] During the liquid phase reducing process, it was found that the morphology and size of Cu_2O nanoparticles were influenced by the reactant concentration and reaction temperature.[10−12] Zhang et al.[13] employed poly(vinylpyrrolidone) (PVP) as the surfactant and synthesized Cu_2O nanoparticles with different shapes by adjusting the PVP concentrations. With the increment of PVP, Cu_2O nanoparticles transformed from cubes to truncated cubes, truncated octahedrons, and finally octahedrons in sequence. It was reported that the excessive surfactant caused aggregation of Cu_2O crystals and resulted in a larger particle size.[14] In addition to the reactant concentrations, the reaction temperature also had significant effects on the reducing reaction. The increase in temperature accelerated the reduction of $Cu(OH)_2$ and contributed to the growth of Cu_2O nanoparticles. It was observed that the Cu_2O nanoparticles transformed from truncated octahedrons to spheres, with the temperature increasing from 70 to 100 °C.[15]

For the conventional liquid phase reducing process, the reactants were usually mixed by stirring in beakers or tank reactors. Compared with the conventional reaction systems on a macroscale, micromixers and microreactors have shown great advantages of high reacting efficiency, precise controllability, and low reagent consumption. Since rapid and uniform mixing can be achieved by micromixers, it is quite promising to utilize micromixers to produce nanoparticles.[16−18] Sugano et al.[19] synthesized gold nanoparticles through a Y-shaped micromixer assisted with two piezoelectric valveless micropumps. By increasing the mixing time, tetrachloroauric acid and sodium citrate could be uniformly mixed, and ultrafine gold nanoparticles were obtained. Kimura et al.[20] employed a baffle micromixer to synthesize lipid nanoparticles. The average size

Received: June 13, 2023
Accepted: July 19, 2023
Published: August 1, 2023

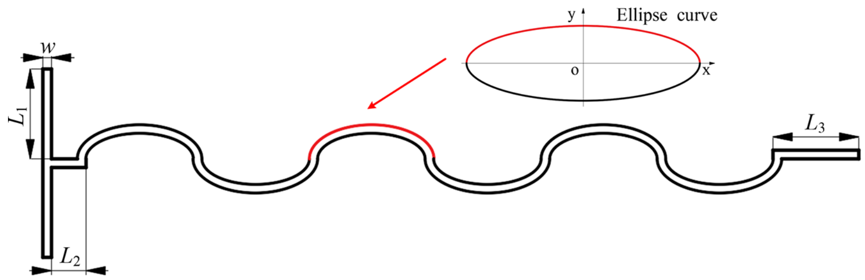

Figure 1. Schematic of the ellipse curve micromixer. Reprinted with permission from ref 27. Copyright 2021 Elsevier.

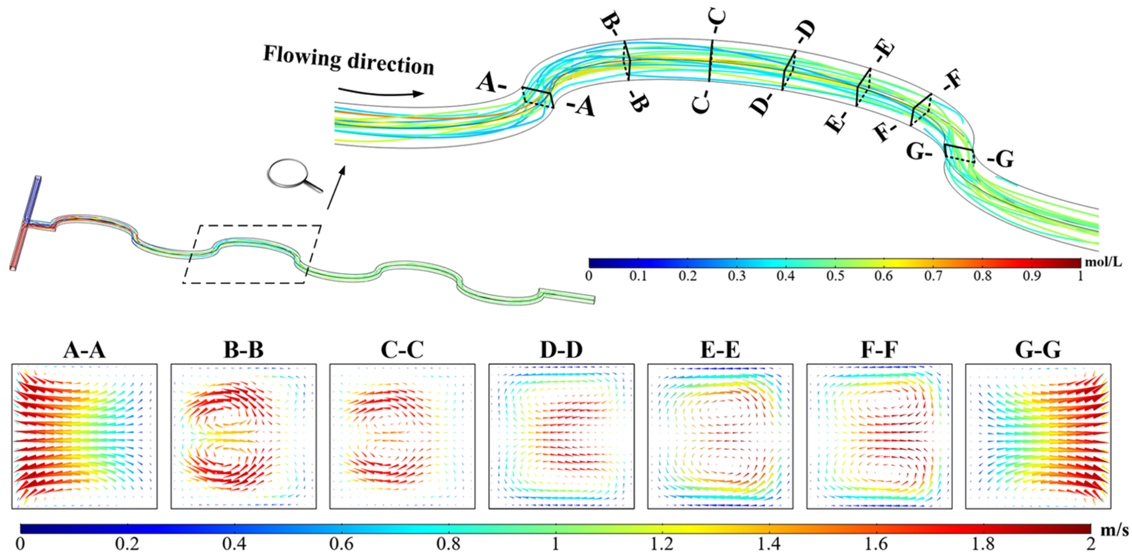

Figure 2. Velocity vectors in cross sections of ellipse curve microchannels at *Re* = 100. Reprinted with permission from ref 27. Copyright 2021 Elsevier.

of lipid nanoparticles was only 10 nm owing to the significant secondary flows. A splitting and recombining micromixer has been used to produce ultrafine hexanitrostilbene.[21] The results showed that the hexanitrostilbene synthesized by micromixer had a smaller size and a narrower size distribution than those synthesized by beakers.

The serpentine structure is one of the most efficient micromixer structures with excellent mixing performance and therefore has been widely used for the synthesis of nanoparticles.[22,23] A serpentine micromixer with sinusoidal microchannels has been employed to produce nanocrystalline cellulose.[24] The nanocrystalline cellulose prepared by the serpentine micromixer had higher yields and narrower size distribution than those prepared by conventional methods. Baruah et al.[25] synthesized ZnO nanoparticles with different shapes by adjusting the geometry of serpentine microchannels. The ZnO nanoparticles changed from spindles to thin sheets with the decrement of microchannel heights. Florez et al.[26] using a serpentine micromixer synthesized magnetite nanoparticles. It was found that the energy consumption of micromixing synthesis was much lower than that of the conventional synthesizing methods.

In this research, an ellipse curve serpentine micromixer that had been proposed in our prior works was adopted to synthesize Cu_2O nanoparticles.[27] Cu_2O nanoparticles were synthesized by both micromixing and stirring in a beaker, with different PVP concentrations and temperatures. The effects of mixing performance on the formation of Cu_2O nanoparticles were investigated. The photocatalytic degradation experiments of Rhodamine B were carried out to investigate the photocatalysis of Cu_2O nanoparticles synthesized under different mixing conditions.

2. EXPERIMENTAL DETAILS

2.1. Ellipse Curve Serpentine Micromixer. The ellipse curve serpentine micromixer employed to synthesize Cu_2O nanoparticles had been proposed in our prior work, as shown in Figure 1. The serpentine microchannels were derived from ellipse curves, which were simple and easy to manufacture. As presented in Figure 2, Dean vortices were generated all along the flow path. An efficient mixing could be achieved through intense and effective chaotic advection. The geometry parameters of the serpentine micromixer are exhibited in Table 1.

Table 1. Geometry Parameters of the Ellipse Curve Micromixer

geometry parameters	value (μm)
inlet length (L_1)	2000
straight channel length (L_2)	800
outlet length (L_3)	1600
channel width (w)	200
channel depth (d)	200
major axis of ellipse (a)	1355
ellipse circumference (C)	6000

https://doi.org/10.1021/acsomega.3c04200
ACS Omega 2023, 8, 29758−29769

Mixing performance (M) is used to evaluate the homogeneity of mixing (0 means absolutely no mixing and 100% means complete mixing). The mixing performance of the micromixer is dependent on the Reynolds number (Re), which is defined as eq 1.

$$Re = \frac{\rho V D_h}{\mu} \quad (1)$$

where V, μ, D_h, and ρ represent the flow velocity, the dynamic viscosity, the hydraulic diameter, and the density of fluids, respectively. Since the mixing fluids under different experimental conditions are the same, the Reynolds number (Re) only represents the flow velocity. The correlation between mixing performance (M) and Reynolds number (Re) is exhibited in Figure 3. As shown, a higher Re corresponds to better mixing performance because the chaotic advection is stronger at the higher flow velocity. Reynolds numbers are set at 30 and 100 in the micromixing synthesis of Cu_2O nanoparticles in order to investigate the formation process of nanoparticles under different mixing conditions.

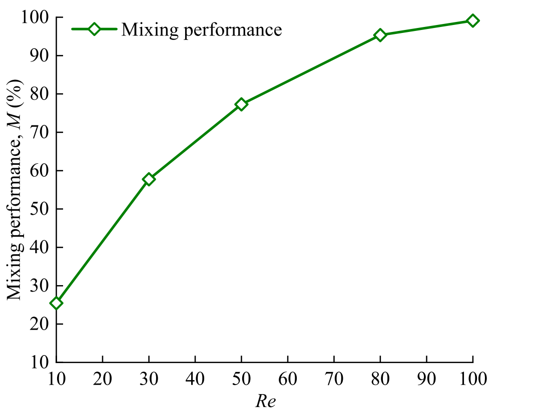

Figure 3. Mixing performance of ellipse curve micromixer with Re from 10 to 100. Reprinted with permission from ref 27. Copyright 2021 Elsevier.

2.2. Synthesis Procedures of Cu_2O Nanoparticles. Cu_2O nanoparticles were synthesized by the ellipse curve micromixer according to Figure 4a. The precursor was $Cu(OH)_2$ and the reducing agent was glucose. A copper sulfate solution was first prepared by dissolving 0.64 g of anhydrous copper sulfate in 25 mL of deionized water. Sodium hydroxide (0.5 g) was dissolved in 25 mL of deionized water to prepare a sodium hydroxide solution. The $Cu(OH)_2$ suspension was prepared by mixing copper sulfate solution and sodium hydroxide solution in a beaker. In addition, 0.36 g of anhydrous glucose was dissolved in 50 mL of deionized water to prepare a glucose solution. The total amount of the reaction solutions was 100 mL. The molar concentration of copper sulfate, sodium hydroxide, and glucose were 0.05, 0.15, and 0.1 mol/L, respectively. The reduction of $Cu(OH)_2$ is described in eq 2.

$$2Cu(OH)_2 + CH_2OH(CHOH)_4CHO \stackrel{\Delta}{=} Cu_2O + CH_2OH(CHOH)_4COOH + 2H_2O \quad (2)$$

Sodium citrate (0.1 g) was added to the sodium hydroxide solution as a chelating agent. Sodium citrate was reported to improve the dispersion of copper hydroxide suspension and help to make the Cu_2O nanoparticles more uniform.[11] Poly(vinylpyrrolidone) (PVP, K-30, 58000) was adopted as the surfactant. The amount of PVP changed from 0.58 to 1.74 g, with the corresponding molar concentration changing from 0.1 to 0.3 mmol/L, as presented in Table 2.

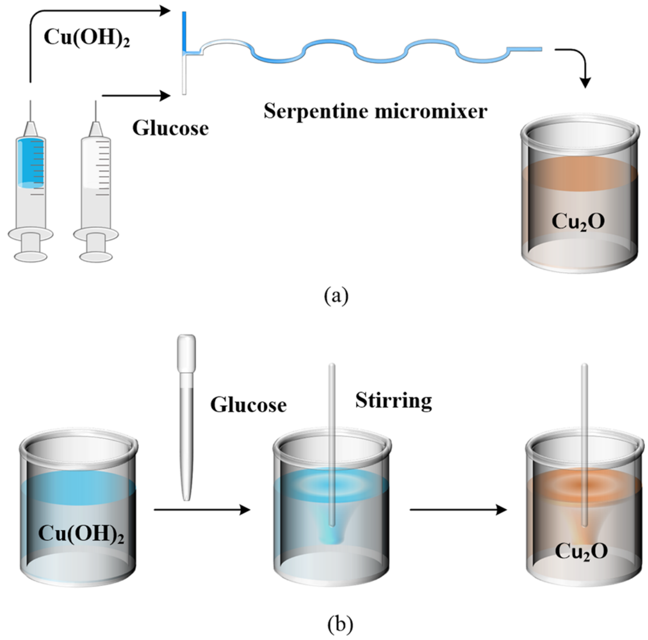

Figure 4. (a) Synthesis of Cu_2O nanoparticles by micromixing. (b) Synthesis of Cu_2O nanoparticles by stirring in a beaker.

Table 2. Experimental Conditions of Synthesizing Cu_2O Nanoparticles

series	molar concentration of PVP (c_{PVP}, mmol/L)
1	0.10
2	0.15
3	0.20
4	0.25
5	0.30

The setup of synthesizing Cu_2O nanoparticles by micromixing is exhibited in Figure 5. The solutions of $Cu(OH)_2$ and glucose were steadily injected into the ellipse curve micromixer by a syringe pump. Products were collected from the outlet and heated in a water bath. The temperature was set at 80 °C in the initial study. For comparative research, Cu_2O nanoparticles were also synthesized by stirring in a beaker under the same experimental conditions, as shown in Figure 4b. The glucose solution was added dropwise to the prepared $Cu(OH)_2$ suspension, and then they were mixed by stirring.

2.3. Photocatalytic Degradation of Rhodamine B. Cu_2O are excellent photocatalysts that have been widely employed for the degradation of organic dyes. The Cu_2O nanoparticles synthesized by micromixing and stirring were used for the degradation of Rhodamine B to investigate their photocatalysis. Cu_2O nanoparticles (0.02 g) were first added in 30 mL of Rhodamine B solutions (5 mg/L). They were stirred in a magnetic stirrer for 40 min under dark conditions to reach the absorption−desorption equilibrium. The solution was then irradiated under an ultraviolet lamp (50 W, wavelength of 365 nm), and 0.1 mL of 30% H_2O_2 solution was added to accelerate the degradation of Rhodamine B. Five milliliters of

https://doi.org/10.1021/acsomega.3c04200
ACS Omega 2023, 8, 29758−29769

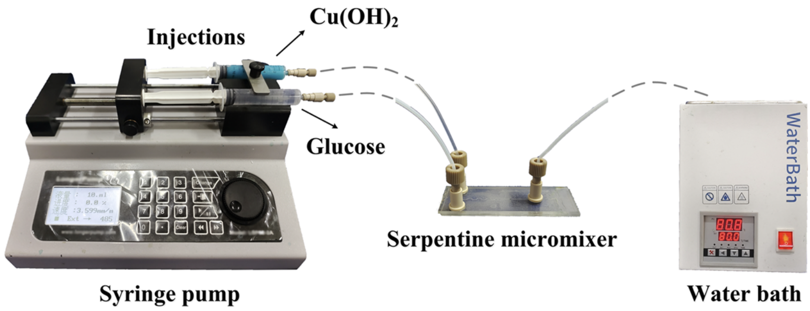

Figure 5. Setup of synthesizing Cu_2O nanoparticles by micromixing.

the reacting solution was taken every 10 min to measure its absorbance. The UV−vis photometer was set at a wavelength of 554 nm, which was the maximum absorbance wavelength of Rhodamine B. The degradation percent (Deg_p) of Rhodamine B was calculated based on eq 3.

$$Deg_p = \left(1 - \frac{A_t}{A_0}\right) \times 100\% \quad (3)$$

where A_t is the absorbance of the solution after irradiating for t mins and A_0 is the absorbance of the solution before the irradiation. The higher degradation percent of Rhodamine B connotes that the used Cu_2O nanoparticles have stronger photocatalysis. Three comparative experiments were conducted. A Rhodamine B solution only added Cu_2O nanoparticles without H_2O_2, while the other one only added H_2O_2 without Cu_2O nanoparticles. A blank experiment without any photocatalysts was carried out on the same condition.

3. RESULTS AND DISCUSSION

3.1. Cu_2O Nanoparticles Synthesized with Different PVP Concentrations. The phase purity of the products was examined by X-ray powder diffraction (XRD), as shown in Figure 6. The reflection peaks of both the products synthesized by micromixing and stirring show the same intensities and positions with the standard card JCPDS No. 05-0667. It means that the products are pure Cu_2O. All three products have sharp and strong reflection peaks, which connotes that they have high crystallinity and there is no impurity.

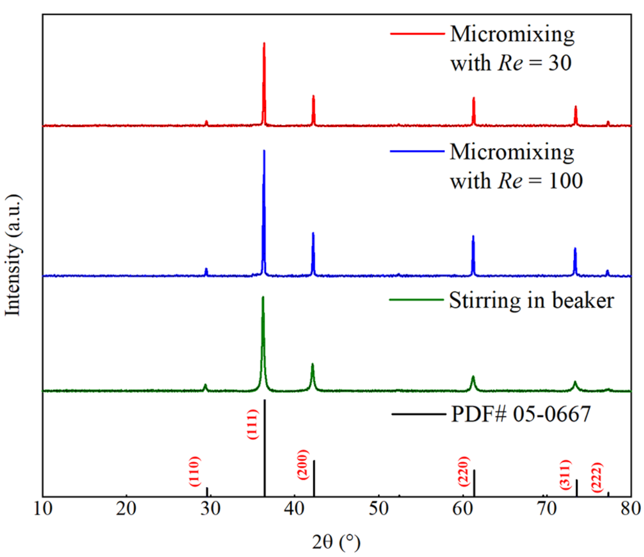

Figure 6. XRD patterns of products synthesized by micromixing and stirring in a beaker.

The three products examined are synthesized with PVP = 0.3 mmol/L at T = 80 °C, and their morphologies are exhibited in Figure 7. The Cu_2O nanoparticles are mainly in the shapes of truncated octahedrons, truncated cubes, and quasi-spheres, corresponding to the three different mixing conditions. The truncated octahedrons have a larger exposed area of the {111} crystal planes than the truncated cubes did, while the exposed crystal planes of quasi-spheres were indistinguishable due to the excessive aggregation of Cu_2O crystals. Therefore, the reflection peaks, especially the {111} peak of Cu_2O nanoparticles synthesized by micromixing with Re = 100, are much higher than those of other products.

The Cu_2O nanoparticles synthesized under the three mixing conditions were analyzed using a scanning electron microscope (SEM). One hundred particles were taken from each synthesizing condition to be measured by the Image J software. The average diameter and standard deviation of Cu_2O nanoparticles synthesized with various PVP concentrations are shown in Figure 8. The size distribution of Cu_2O nanoparticles synthesized by micromixing and stirring are compared in Figure 9.

As presented in Figure 8, for Cu_2O nanoparticles synthesized by micromixing, both the average diameter and standard deviation decrease with PVP increasing from 0.1 to 0.25 mmol/L. The smallest and most uniform Cu_2O nanoparticles are obtained at PVP = 0.25 mmol/L. Nevertheless, the average diameter and standard deviation increase with the further increase of PVP. As shown in Figure 9d, for Cu_2O nanoparticles synthesized by micromixing at Re = 30, the nanoparticles are mainly distributed in the two ranges of 150−300 and 300−450 nm, and only a small number of nanoparticles are larger than 450 nm when the PVP concentration was 0.25 mmol/L. With the PVP concentration increasing to 0.3 mmol/L, there are fewer nanoparticles distributed in the range of 150−300 nm, and the number of nanoparticles with diameters above 450 nm increases significantly, as shown in Figure 9e. It indicates that the Cu_2O nanoparticles are coarsened and their homogeneity becomes worse.

For Cu_2O nanoparticles synthesized by stirring in a beaker, the smallest and most uniform nanoparticles are obtained at PVP = 0.15 mmol/L, as seen in Figure 8. With the further increase of PVP, the average diameter and standard deviation increase, which is similar to the Cu_2O nanoparticles synthesized by micromixing. It reflects that the size of Cu_2O nanoparticles first decreases and then increases with the increase of PVP, whether the Cu_2O nanoparticles are synthesized by micromixing or stirring. PVP can be adsorbed

https://doi.org/10.1021/acsomega.3c04200
ACS Omega 2023, 8, 29758−29769

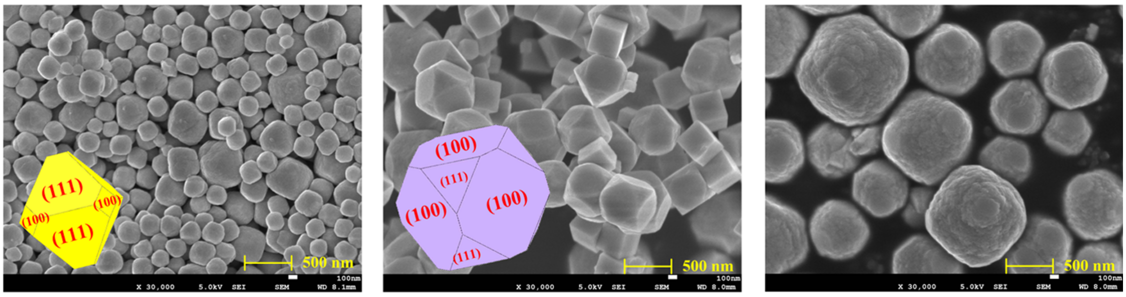

(a) Micromixing with $Re = 100$ (b) Micromixing with $Re = 30$ (c) Stirring in beaker

Figure 7. Morphologies of Cu_2O nanoparticles synthesized by micromixing and stirring in a beaker.

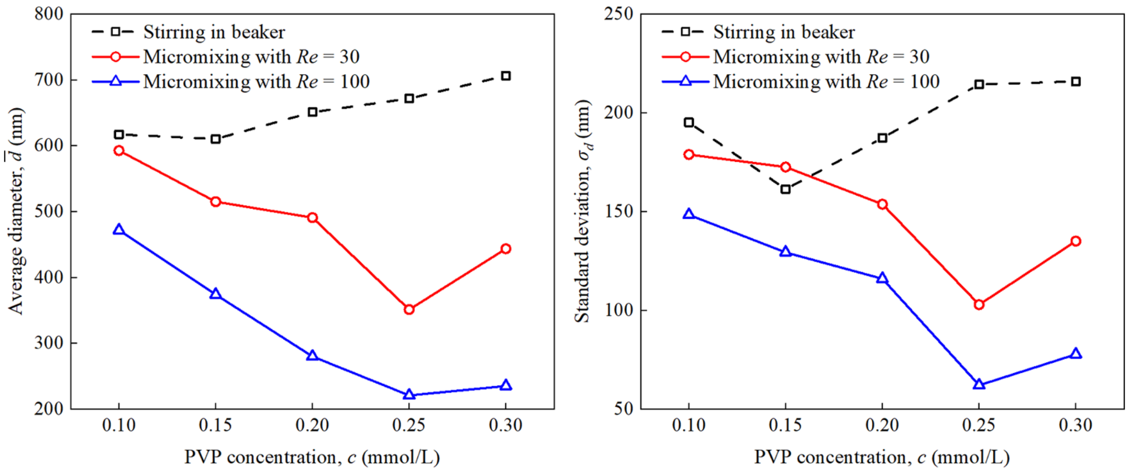

(a) (b)

Figure 8. (a) Average diameter and (b) standard deviation of Cu_2O nanoparticles synthesized by micromixing and stirring with various PVP concentrations.

on the Cu_2O crystal planes to hinder crystal growth. Therefore, smaller Cu_2O nanoparticles can be obtained by adding PVP. However, the PVP absorbed on Cu_2O crystal planes would stick to each other when excessive PVP is added, leading to the aggregation of Cu_2O crystals. At the same time, the irregular aggregation of Cu_2O crystals also increases the difference in particle sizes, which causes the deterioration of particle homogeneity.

3.2. Formation Process of Cu_2O Nanoparticles under Different Mixing Conditions. In addition to the reactant concentrations, the mixing conditions of reactants have significant effects on the size and morphology of nanoparticles. On the one hand, it is seen from Figure 8 that the Cu_2O nanoparticles synthesized by micromixing are finer and more uniform than those synthesized by stirring in a beaker. On the other hand, the Cu_2O nanoparticles synthesized at $Re = 100$ are finer than those synthesized at $Re = 30$, although the sizes of Cu_2O nanoparticles synthesized by micromixing at $Re = 30$ and 100 display similar variation trends. As presented in Figure 9, the Cu_2O nanoparticles synthesized at $Re = 100$ are mainly distributed in the range from 150 to 300 nm when PVP $\geq$ 0.2 mmol/L, while the Cu_2O nanoparticles synthesized at $Re = 30$ are distributed in a wider range from 150 to 450 nm.

The formation process of Cu_2O nanoparticles synthesized by micromixing and stirring is delineated in Figure 10. For the stirring synthesis that proceeds in macroscopic volume, it takes a period of time for $Cu(OH)_2$ and glucose to achieve adequate mixing so that the reduction of $Cu(OH)_2$ is insufficient at the beginning stage. As shown in Figure 10c, reduced Cu_2O, unreacted $Cu(OH)_2$, and glucose coexist in the beaker. The subsequent $Cu(OH)_2$ is still in the reduction process when the initially reduced Cu_2O nucleates. Different stages of Cu_2O exist in the same space, including the newly nucleated Cu_2O crystals, the growing Cu_2O crystals, and the unnucleated Cu_2O. When $Cu(OH)_2$ is fully reduced, the sizes of Cu_2O crystals distribute in a wide range. The Cu_2O nanoparticles finally synthesized have poor homogeneity.

Compared with the conventional stirring synthesis, the rapid and complete mixing between $Cu(OH)_2$ and glucose can be achieved by the ellipse curve micromixer. As shown in Figure 10a, the reduction of $Cu(OH)_2$ is quite sufficient at $Re = 100$ owing to the excellent mixing performance, nearly 100%. The copper elements are mainly present as high concentration of Cu_2O molecules with little unreduced $Cu(OH)_2$. The subsequent reduced Cu_2O flowing into the vessel will aggregate on the initially nucleated Cu_2O crystals. The Cu_2O crystals are almost at the same stage when $Cu(OH)_2$ is fully reduced. Therefore, the Cu_2O nanoparticles finally obtained are uniform in size.

The mixing performance is less than 60% when $Re = 30$ and thus the reduction of $Cu(OH)_2$ at $Re = 30$ is not as sufficient as that at $Re = 100$. Unreduced $Cu(OH)_2$ coexists with the reduced Cu_2O in the vessel, as seen in Figure 10b. Some Cu_2O is just reduced, while the formed Cu_2O crystals grow. The homogeneity of Cu_2O nanoparticles synthesized at $Re = 30$ is worse than those synthesized at $Re = 100$. Nevertheless, the

https://doi.org/10.1021/acsomega.3c04200
ACS Omega 2023, 8, 29758−29769

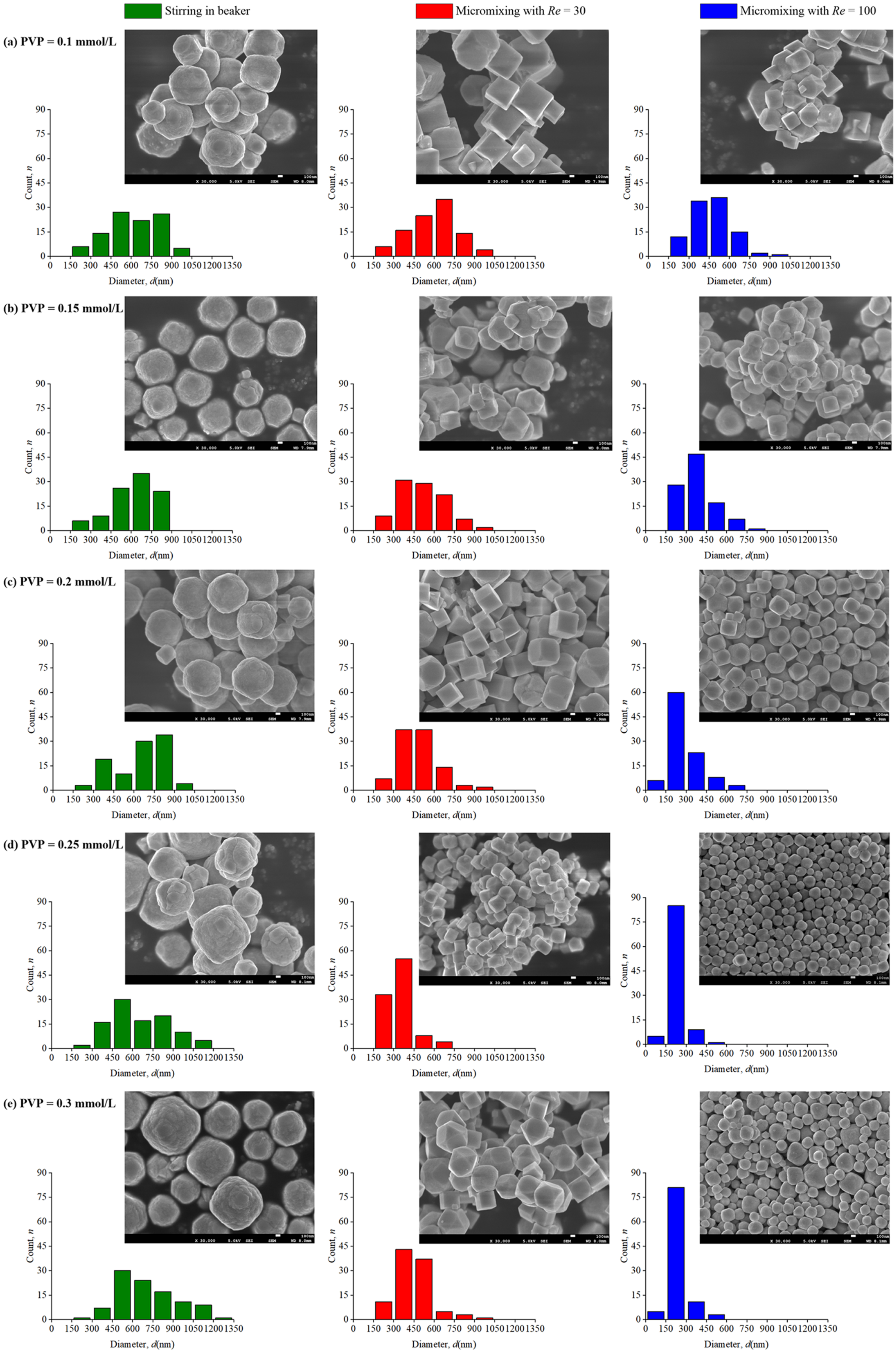

Figure 9. Size distribution of Cu_2O nanoparticles synthesized by micromixing and stirring with various PVP concentrations.

reduction of $Cu(OH)_2$ at Re = 30 is still more sufficient than the stirring synthesis. The Cu_2O nanoparticles synthesized by micromixing at Re = 30 are more uniform compared with those synthesized by stirring.

https://doi.org/10.1021/acsomega.3c04200
ACS Omega 2023, 8, 29758−29769

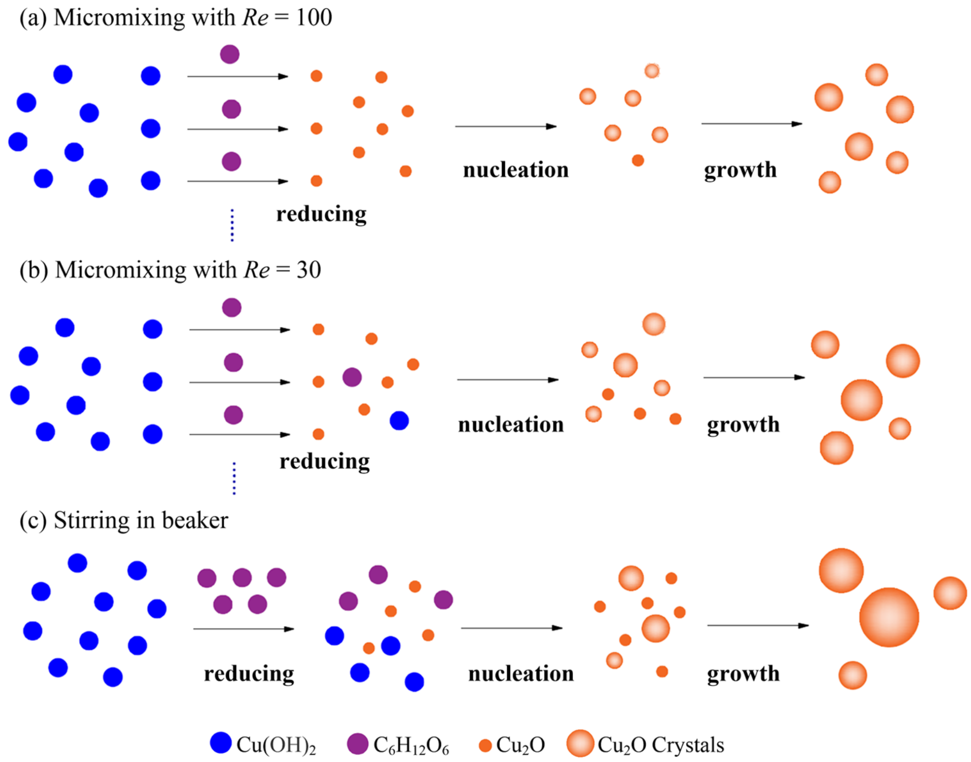

Figure 10. Formation of Cu_2O nanoparticles synthesized by micromixing and stirring in a beaker.

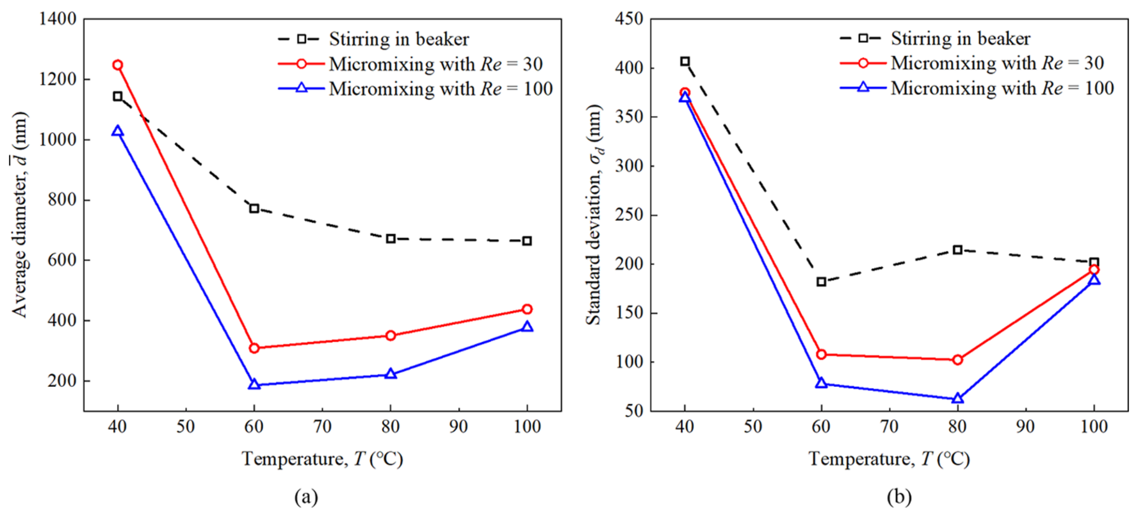

Figure 11. (a) Average diameter and (b) standard deviation of Cu_2O nanoparticles synthesized by micromixing and stirring with various temperatures.

The Cu_2O concentration is high for the micromixing synthesis, since the excellent mixing performance brings about sufficient reduction of $Cu(OH)_2$. A large number of Cu_2O crystals are nucleated to consume the reduced Cu_2O. By contrast, the Cu_2O concentration is relatively low for the stirring synthesis due to the insufficient reduction of $Cu(OH)_2$. Fewer Cu_2O crystals are formed in the stirring synthesis. Therefore, the Cu_2O nanoparticles synthesized by micromixing are finer than those synthesized by stirring in a beaker because the total amount of Cu_2O is the same.

A similar phenomenon has also been reported by Bai et al.[10] They found that the increase in the stirring rates contributed to the hindered aggregation of Cu_2O crystals. The size of Cu_2O nanoparticles decreased from 800 to 150 nm with the stirring rates increasing from 4 to 6 r/s. The size of Cu_2O nanoparticles synthesized by micromixing with Re = 100 at PVP $\geq$ 0.25 mmol was nearly 200 nm, which was close to that of the Cu_2O nanoparticles obtained at a stirring rate of 5 r/s. However, Bai et al.[10] neglected the influence of mixing performance on the reducing reactions. The increase of stirring rates played a similar role to a micromixer, which improved the mixing among solutions and led to the more sufficient reduction of $Cu(OH)_2$.

In addition to the nanoparticle sizes, the morphology of Cu_2O nanoparticles is also influenced by the mixing conditions. As shown in Figure 7, the Cu_2O nanoparticles synthesized by micromixing with the Re = 100 are mainly truncated octahedrons. When Re = 100, rapid and uniform

https://doi.org/10.1021/acsomega.3c04200
ACS Omega 2023, 8, 29758−29769

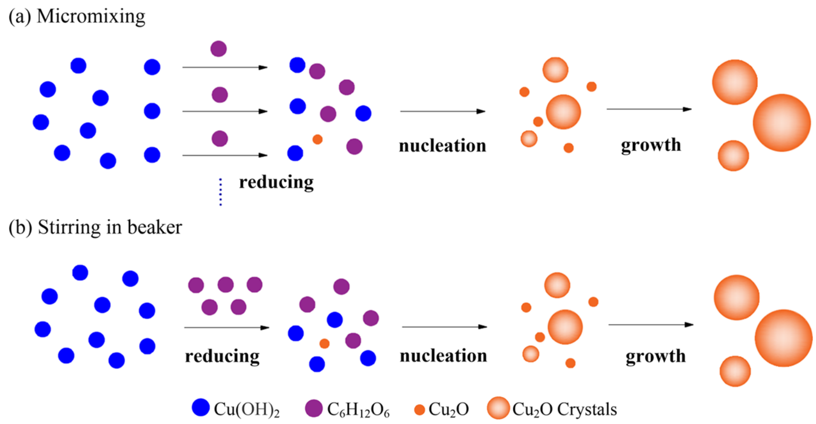

Figure 12. Formation of Cu_2O nanoparticles by micromixing and stirring in a beaker at T = 40 °C.

mixing is achieved among the whole reactants including $Cu(OH)_2$, glucose, and PVP. The PVP can be sufficiently in contact with the Cu_2O crystals. The PVP first covers the {100} crystal planes to hinder the crystal growth in the {100} plane direction. Then, there is also much PVP absorbed on the {111} crystal planes to hinder the crystal growth in the {111} plane direction. As a result, the exposed area of the {111} crystal plane becomes larger, while the exposed area of the {100} crystal plane becomes relatively smaller. The Cu_2O nanoparticles in the shape of truncated octahedrons are finally formed.

When Re = 30, the mixing among $Cu(OH)_2$, glucose, and PVP is not as uniform as the mixing at Re = 100. The contact between PVP and Cu_2O crystals is relatively insufficient. Only a small amount of PVP can be absorbed on the {111} crystal planes after covering the {100} crystal planes. Therefore, the Cu_2O nanoparticles obtained are truncated cubes, which have a larger exposed area of the {100} crystal planes. However, for the stirring synthesis, there are heavy irregular collisions and aggregations among the Cu_2O crystals. The Cu_2O nanoparticles synthesized are large quasi-spheres, of which the dominated crystal plane is indistinguishable.

3.3. Effects of Temperature on the Synthesis of Cu_2O Nanoparticles. Extended research has been carried out to reveal the effects of temperature on the synthesis of Cu_2O nanoparticles, since temperature is a considerable factor that affects the nucleation and growth of Cu_2O crystals. Cu_2O nanoparticles were synthesized by the ellipse curve micromixer with another three temperatures of 40, 60, and 100 °C. The PVP concentration was fixed at 0.25 mmol/L. The Reynolds numbers of micromixing synthesis were settled as 30 and 100, and there were Cu_2O nanoparticles synthesized by stirring in a beaker under the same condition. The average diameter and standard deviation of Cu_2O nanoparticles synthesized with various temperatures are exhibited in Figure 11.

It is seen from Figure 11 that the Cu_2O nanoparticles synthesized by micromixing are finer and more uniform than those synthesized by stirring when T > 40 °C, but the sizes of Cu_2O nanoparticles synthesized by micromixing are similar to those synthesized by stirring when T = 40 °C. The average diameter and standard deviation of Cu_2O nanoparticles synthesized at T = 40 °C are quite large, irrespective of whether the nanoparticles are synthesized by micromixing or by stirring.

The formation process of Cu_2O nanoparticles synthesized at T = 40 °C is presented in Figure 12. The temperature of 40 °C is so low that the reduction of $Cu(OH)_2$ is slow and insufficient. Even though the rapid and complete mixing of $Cu(OH)_2$ and glucose can be achieved through the ellipse curve micromixer, the reduction of $Cu(OH)_2$ is still insufficient. On the one hand, it can be seen from Figure 12 that reduced Cu_2O, unreduced $Cu(OH)_2$ and glucose coexist in the vessel for both the micromixing synthesis and stirring synthesis. Different stages of Cu_2O exist in the same space when $Cu(OH)_2$ is fully reduced and the sizes of Cu_2O crystals distribute in a wide range. As a result, the homogeneity of Cu_2O nanoparticles synthesized at T = 40 °C was poor.

On the other hand, the concentration of Cu_2O is low since the reduction of $Cu(OH)_2$ is slow and insufficient at T = 40 °C. Therefore, fewer Cu_2O crystals are formed and the nanoparticle size becomes larger, compared with the case of T ≥ 60 °C. A similar phenomenon has also been observed by Karmakar in the synthesis of Cu_2O nanoparticles by annealing.[12] They found that the reduction reaction was severely hindered at low annealing temperatures so that only a small amount of Cu_2O was produced. The Cu_2O nanoparticles obtained at low temperatures were larger and more irregular than those obtained at a higher temperature.

As presented in Figure 11, the average diameter and standard deviation decrease dramatically for both the Cu_2O nanoparticles synthesized by micromixing and stirring, when T increases to 60 °C. This is ascribed to the accelerated reduction of $Cu(OH)_2$ with increasing temperature. The concentration of Cu_2O increases rapidly and more Cu_2O crystals are nucleated as the reduction of $Cu(OH)_2$ becomes more sufficient. A large number of Cu_2O nanoparticles with fine and uniform sizes are synthesized. The size distribution of Cu_2O nanoparticles synthesized by micromixing and stirring are compared in Figure 13.

Obviously, the increment in the homogeneity and the decrement in the size of Cu_2O nanoparticles synthesized by micromixing are more significant than those synthesized by stirring in a beaker because the mixing is more efficient in the micromixer. As shown in Figure 13b, for the Cu_2O nanoparticles synthesized by micromixing at Re = 100, 90% of the nanoparticles are smaller than 300 nm when T = 60 °C. In addition, the nanoparticle size also reached the minimum when T increases to 60 °C, as seen in Figure 11a.

The size of Cu_2O nanoparticles synthesized by micromixing increases while the standard deviation decreases to the lowest when T increases to 80 °C. As seen from Figure 13b,c, for Cu_2O nanoparticles synthesized by micromixing at Re = 100,

https://doi.org/10.1021/acsomega.3c04200
ACS Omega 2023, 8, 29758−29769

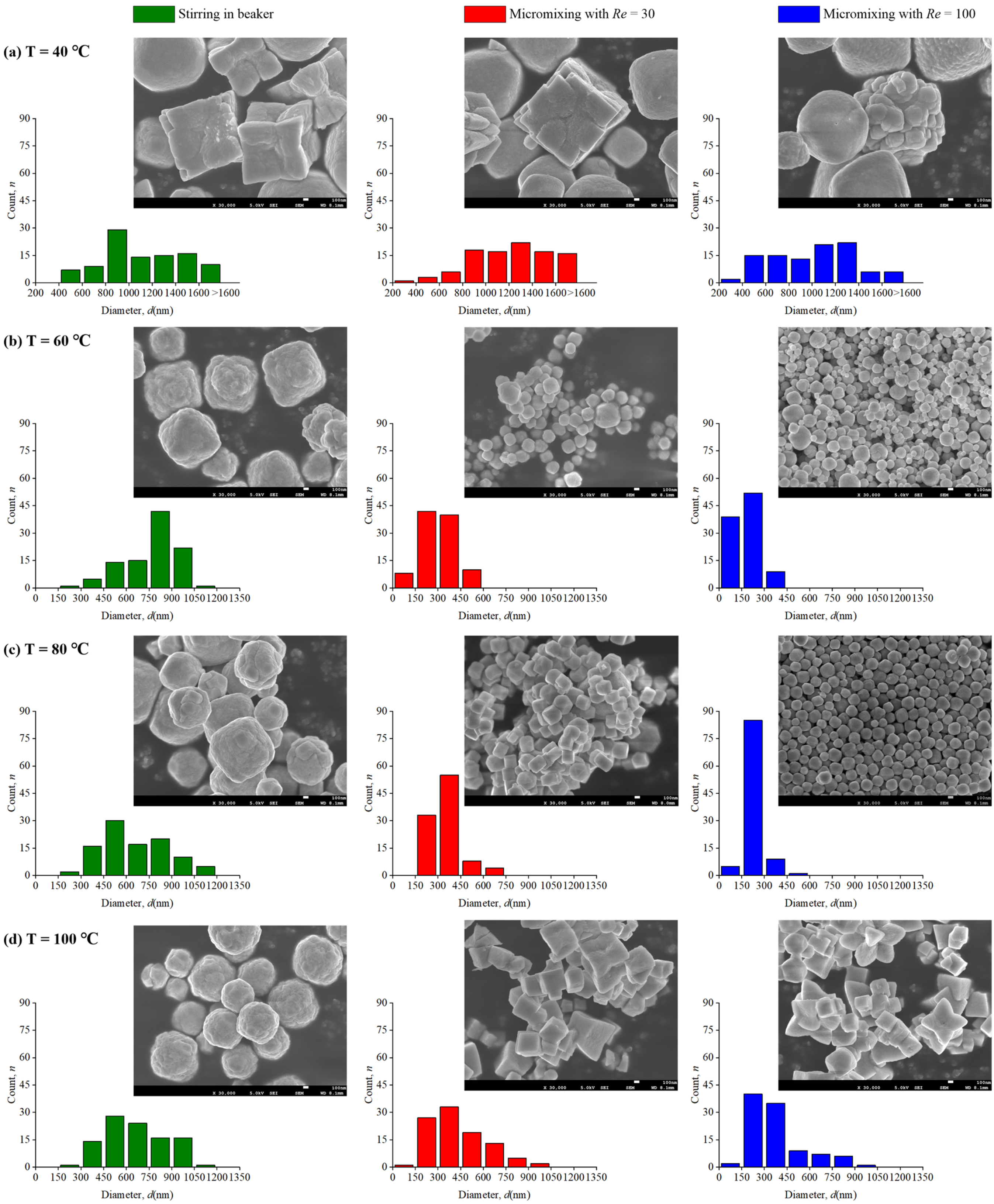

Figure 13. Size distribution of Cu_2O nanoparticles synthesized by micromixing and stirring at various temperatures.

the number of nanoparticles with diameters lower than 150 nm is significantly reduced. More nanoparticles are distributed in a narrower range from 150 to 300 nm. This change can be interpreted by Ostwald ripening. As displayed in Figure 14, the small nucleated Cu_2O crystals first dissolve in the solution, and then the Cu_2O would aggregate on the large nucleated Cu_2O crystals when T increases from 60 to 80 °C. As a result, the Cu_2O nanoparticles become larger but more uniform.

As presented in Figure 11, both the average diameter and standard deviation of Cu_2O nanoparticles synthesized by

https://doi.org/10.1021/acsomega.3c04200
ACS Omega 2023, 8, 29758−29769

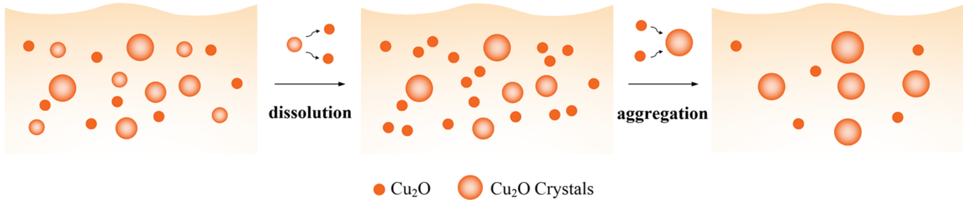

Figure 14. Ostwald ripening of Cu_2O nanoparticles by micromixing when T increases from 60 to 80 °C.

micromixing increase with T further increasing to 100 °C. On the one hand, Ostwald ripening is stronger when T = 100 °C. It can be seen from Figure 13d that there are more Cu_2O nanoparticles with diameters larger than 450 nm. On the other hand, the molecular motion of Cu_2O becomes more intense at T = 100 °C, resulting in the irregular aggregation of Cu_2O crystals. A number of Cu_2O nanoparticles with irregular shapes are formed and the homogeneity of nanoparticles is deteriorated.

For the Cu_2O nanoparticles synthesized by stirring, the increase in temperature improves the mixing between $Cu(OH)_2$ and glucose and simultaneously accelerates the reduction of $Cu(OH)_2$. As shown in Figure 11a, the average diameter of Cu_2O nanoparticles decreases with T increasing from 40 to 60 °C. However, the reduction of $Cu(OH)_2$ in the stirring synthesis is not as sufficient as that in the micromixing synthesis, although the mixing by stirring is enhanced when T > 40 °C. The Cu_2O nanoparticles synthesized by micromixing are still finer and more uniform than those synthesized by stirring in a beaker when T > 40 °C.

3.4. Photocatalysis of Cu_2O Nanoparticles. Photocatalysis of the synthesized Cu_2O nanoparticles has been investigated through the photocatalytic degradation experiments of Rhodamine B. The synthesizing conditions of the Cu_2O nanoparticles used in the degradation experiments are presented in Table 3, and their morphologies are exhibited in Figure 7. The degradation percent (Deg_p) of Rhodamine B with different Cu_2O nanoparticles is shown in Figure 15.

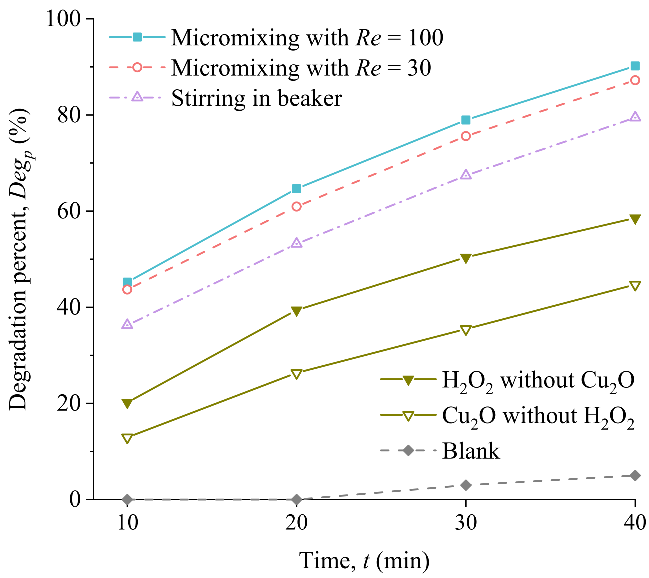

Figure 15. Degradation percent of Rhodamine B with different Cu_2O nanoparticles.

Table 3. Cu_2O Nanoparticles for the Photocatalytic Degradation of Rhodamine B

series	average diameter (nm)	synthesizing method	PVP concentration (mmol/L)	temperature (°C)
1	235	micromixing at Re = 100	0.3	80
2	443	micromixing at Re = 30	0.3	80
3	706	stirring in beaker	0.3	80

The Cu_2O nanoparticles show excellent photocatalysis for the degradation of Rhodamine B, as seen in Figure 15. Rhodamine B hardly degrades without the addition of photocatalysts. The degradation percent of Rhodamine B approaches 90% after 40 min with the Cu_2O nanoparticles synthesized by micromixing. The degradation percent is more than 70% after 40 min with the Cu_2O nanoparticles synthesized by stirring. It indicates that the Cu_2O nanoparticles synthesized by micromixing have better photocatalysis than those synthesized by stirring.

One of the reasons is that the Cu_2O nanoparticles synthesized by micromixing have a larger exposed area of {111} crystal planes. According to the work of Ho and Huang, the {111} crystal planes have better photocatalysis than the {100} crystal planes.[28] Since there are dangling bonds on the {111} crystal plane, the {111} plane is more active to interact with the other molecules. By contrast, Cu atoms are coordinated and saturated on the {100} crystal plane. The {100} plane is electrically neutral and is inactive to interact with other molecules. Therefore, the truncated octahedrons have better photocatalysis than the truncated cubes.

On the other hand, the Cu_2O nanoparticles with a smaller size are more favorable for the photocatalytic degradation of Rhodamine B. This is because the smaller Cu_2O nanoparticles have a larger specific surface area. The electron−hole pairs produced under irradiation have a larger area in contact with Rhodamine B, which promotes the degradation of Rhodamine B.

As presented in Figure 15, the degradation percent of Rhodamine B is only 40% after 40 min without the addition of H_2O_2. It is similar to the work by Pang et al.,[6] in which only 80% Rhodamine B was degraded after 180 min. The poor and weakened photocatalysis is caused by the recombination of electron−hole pairs. The photogenerated electron−hole pairs are unstable and easy to recombine. The H_2O_2 added can receive the photogenerated electrons produced by the Cu_2O nanoparticles so that the recombination of electron−hole pairs is hindered. The addition of H_2O_2 improves the photocatalysis of Cu_2O and makes it more stable. On the other hand, the hydroxyl radicals produced by H_2O_2 have a strong oxidization property, which further enhances the photocatalytic degradation of Rhodamine B.

https://doi.org/10.1021/acsomega.3c04200
ACS Omega 2023, 8, 29758−29769

4. CONCLUSIONS

A method to synthesize Cu_2O nanoparticles utilizing the ellipse curve serpentine micromixer is put forward. The difference in the formation process of Cu_2O nanoparticles between micromixing synthesis and stirring synthesis is first elucidated. The excellent mixing performance of the micromixer brings about a sufficient reduction of $Cu(OH)_2$. Therefore, the Cu_2O nanoparticles synthesized by micromixing are finer and more uniform compared with the Cu_2O nanoparticles synthesized by stirring on the same condition. The Cu_2O nanoparticles synthesized at $Re = 100$ have a smaller size and a narrower size distribution than those synthesized at $Re = 30$, since the reduction of $Cu(OH)_2$ is more sufficient at a higher Re. The smallest Cu_2O nanoparticles are obtained at $T = 60$ °C, while the most uniform Cu_2O nanoparticles are obtained at $T = 80$ °C owning to the Ostwald ripening. The photocatalytic degradation experiments of Rhodamine B show that the Cu_2O nanoparticles synthesized by micromixing have better photocatalysis than those synthesized by stirring. This is because the Cu_2O nanoparticles synthesized by micromixing are smaller in size and have a larger exposed area of the {111} crystal planes. It is demonstrated that the micromixing synthesis was more suitable for the production of Cu_2O nanoparticles with efficient photocatalysis.

AUTHOR INFORMATION

Corresponding Author

Zhanqiang Liu − *School of Mechanical Engineering, Shandong University, Jinan 250061 Shandong, China; Key Laboratory of High Efficiency and Clean Mechanical Manufacture of MOE/Key National Demonstration Center for Experimental Mechanical Engineering Education, Jinan 250061 Shandong, China*; orcid.org/0000-0002-4790-0052; Phone: +86-531-88393206; Email: melius@sdu.edu.cn; Fax: +86-531-88392045

Authors

Xin Wang − *School of Mechanical Engineering, Shandong University, Jinan 250061 Shandong, China; Key Laboratory of High Efficiency and Clean Mechanical Manufacture of MOE/Key National Demonstration Center for Experimental Mechanical Engineering Education, Jinan 250061 Shandong, China*

Yukui Cai − *School of Mechanical Engineering, Shandong University, Jinan 250061 Shandong, China; Key Laboratory of High Efficiency and Clean Mechanical Manufacture of MOE/Key National Demonstration Center for Experimental Mechanical Engineering Education, Jinan 250061 Shandong, China*

Qinghua Song − *School of Mechanical Engineering, Shandong University, Jinan 250061 Shandong, China; Key Laboratory of High Efficiency and Clean Mechanical Manufacture of MOE/Key National Demonstration Center for Experimental Mechanical Engineering Education, Jinan 250061 Shandong, China*

Bing Wang − *School of Mechanical Engineering, Shandong University, Jinan 250061 Shandong, China; Key Laboratory of High Efficiency and Clean Mechanical Manufacture of MOE/Key National Demonstration Center for Experimental Mechanical Engineering Education, Jinan 250061 Shandong, China*

Complete contact information is available at: https://pubs.acs.org/10.1021/acsomega.3c04200

Notes

The authors declare no competing financial interest.

ACKNOWLEDGMENTS

The author would like to acknowledge the financial support from the National Key Research and Development Program of China (2019YFB2005401). This work was also supported by grants from the National Natural Science Foundation of China (No. 91860207), the Shandong Provincial Key Research and Development Program (Major Scientific and Technological Innovation Project-2020CXGC010204), and the Taishan Scholar Foundation.

REFERENCES

(1) Singh, A.; Ahmed, A.; Prasad, K. N.; Khanduja, S.; Singh, S. K.; Srivastava, J. K.; Gajbhiye, N. S. Antibiofilm and membrane-damaging potential of cuprous oxide nanoparticles against Staphylococcus aureus with reduced susceptibility to vancomycin. *Antimicrob. Agents Chemother.* **2015**, *59*, 6882−6890.

(2) Zhang, J. L. J.; Liu, J.; Peng, Q.; Peng, Q.; Wang, X.; Wang, X.; Li, Y. Nearly monodisperse Cu_2O and CuO nanospheres: preparation and applications for sensitive gas sensors. *Chem. Mater.* **2006**, *18*, 867−871.

(3) Zhang, Z.; Wu, H.; Yu, Z.; Song, R.; Qian, K.; Chen, X.; Tian, J.; Zhang, W.; Huang, W. Site-resolved Cu_2O catalysis in the oxidation of CO. *Angew. Chem., Int. Ed.* **2019**, *58*, 4276−4280.

(4) Han, Y.; Meng, Z.; Wu, Y.; Zhang, S.; Wu, S. Structural Colored Fabrics with Brilliant Colors, Low Angle Dependence, and High Color Fastness Based on the Mie Scattering of Cu_2O Spheres. *ACS Appl. Mater. Interfaces* **2021**, *13*, 57796−57802.

(5) Xu, Y.-T.; Guo, Y.; Li, C.; Zhou, X.-Y.; Tucker, M. C.; Fu, X.-Z.; Sun, R.; Wong, C.-P. Graphene oxide nano-sheets wrapped Cu_2O microspheres as improved performance anode materials for lithium ion batteries. *Nano Energy* **2015**, *11*, 38−47.

(6) Pang, H.; Gao, F.; Lu, Q. Glycine-assisted double-solvothermal approach for various cuprous oxide structures with good catalytic activities. *CrystEngComm* **2010**, *12*, 406−412.

(7) Su, X.; Chen, W.; Han, Y.; Wang, D.; Yao, J. In-situ synthesis of Cu_2O on cotton fibers with antibacterial properties and reusable photocatalytic degradation of dyes. *Appl. Surf. Sci.* **2021**, *536*, No. 147945.

(8) Chen, X.; Cui, K.; Hai, Z.; Kuang, W.; Wang, L.; Zhang, J.; Tian, X. Hydrothermal synthesis of Cu_2O with morphology evolution and its effect on visible-light photocatalysis. *Mater. Lett.* **2021**, *297*, No. 129921.

(9) Ma, P. D.; Teng, Z. H.; Hao, Q. L.; Kang, R. N.; Li, B.; Bin, F.; Dou, B. J. Effects of precursor concentration on morphologies of Cu_2O micro/nanocrystals and properties of CO self-sustained catalytic combustion. *Fuel* **2021**, *289*, No. 119776.

(10) Bai, Y. K.; Yang, T. F.; Gu, Q.; Cheng, G. A.; Zheng, R. T. Shape control mechanism of cuprous oxide nanoparticles in aqueous colloidal solutions. *Powder Technol.* **2012**, *227*, 35−42.

(11) Chang, I. C.; Chen, P. C.; Tsai, M. C.; Chen, T. T.; Yang, M. H.; Chiu, H. T.; Lee, C. Y. Large-scale synthesis of uniform Cu_2O nanocubes with tunable sizes by in-situ nucleation. *CrystEngComm* **2013**, *15*, 2363−2366.

(12) Karmakar, S.; Biswas, S.; Kumbhakar, P. Optical, structural, and catalytic properties of synthesized Cu_2O nanocubes. *Indian J. Phys.* **2021**, *95*, 607−619.

(13) Zhang, D.-F.; Zhang, H.; Guo, L.; Zheng, K.; Han, X.-D.; Zhang, Z. Delicate control of crystallographic facet-oriented Cu_2O nanocrystals and the correlated adsorption ability. *J. Mater. Chem.* **2009**, *19*, 5220−5225.

(14) Gou, L.; Murphy, C. J. Solution-phase synthesis of Cu_2O nanocubes. *Nano Lett.* **2003**, *3*, 231−234.

(15) Sui, Y.; Fu, W.; Yang, H.; Zeng, Y.; Zhang, Y.; Zhao, Q.; Li, Y.; Zhou, X.; Leng, Y.; Li, M.; Zhou, G. Low temperature synthesis of Cu_2O crystals: shape evolution and growth mechanism. *Cryst. Growth Des.* **2010**, *10*, 99−108.
(16) Liu, Y.; Jiang, X. Why microfluidics? Merits and trends in chemical synthesis. *Lab Chip* **2017**, *17*, 3960−3978.
(17) Hao, N.; Nie, Y.; Zhang, J. X. J. Microfluidic synthesis of functional inorganic micro-/nanoparticles and applications in biomedical engineering. *Int. Mater. Rev.* **2018**, *63*, 461−487.
(18) Zardi, P.; Carofiglio, T.; Maggini, M. Mild microfluidic approaches to Oxide nanoparticles synthesis. *Chem. - Eur. J.* **2022**, *28*, No. 202103132.
(19) Sugano, K.; Uchida, Y.; Ichihashi, O.; Yamada, H.; Tsuchiya, T.; Tabata, O. Mixing speed-controlled gold nanoparticle synthesis with pulsed mixing microfluidic system. *Microfluid. Nanofluid.* **2010**, *9*, 1165−1174.
(20) Kimura, N.; Maeki, M.; Sato, Y.; Note, Y.; Ishida, A.; Tani, H.; Harashima, H.; Tokeshi, M. Development of the iLiNP Device: Fine Tuning the Lipid Nanoparticle Size within 10 nm for Drug Delivery. *ACS Omega* **2018**, *3*, 5044−5051.
(21) Zhao, S.; Chen, C.; Zhu, P.; Xia, H.; Shi, J.; Yan, F.; Shen, R. Passive micromixer platform for size-and shape-controllable preparation of ultrafine HNS. *Ind. Eng. Chem. Res.* **2019**, *58*, 16709−16718.
(22) Hong, S. O.; Park, K.; Kim, D.; Lee, S. S.; Lee, C.; Kim, J. M. Gear-shaped micromixer for synthesis of silica particles utilizing inertio-elastic flow instability. *Lab Chip* **2021**, *21*, 513−552.
(23) Gan, Z.; Liu, H.; Wang, Y.; Tao, T.; Zhao, M.; Qin, J. One-Step Generation of Porous GelMA Microgels by Droplet-Based Chaotic Advection Effect. *Adv. Mater. Technol.* **2023**, *8*, No. 2201102.
(24) Wang, S.; Zeng, J.; Cheng, Z.; Yuan, Z.; Wang, X.; Wang, B. Precisely controlled preparation of uniform nanocrystalline cellulose via microfluidic technology. *J. Ind. Eng. Chem.* **2022**, *106*, 77−85.
(25) Baruah, A.; Jindal, A.; Acharya, C.; Prakash, B.; Basu, S.; Ganguli, A. K. Microfluidic reactors for the morphology controlled synthesis and photocatalytic study of ZnO nanostructures. *J. Micromech. Microeng.* **2017**, *27*, No. 035013.
(26) Florez, S. L.; Campaña, A. L.; Noguera, M. J.; Quezada, V.; Fuentes, O. P.; Cruz, J. C.; Osma, J. F. CFD Analysis and Life Cycle Assessment of Continuous Synthesis of Magnetite Nanoparticles Using 2D and 3D Micromixers. *Micromachines* **2022**, *13*, 970.
(27) Wang, X.; Liu, Z.; Cai, Y.; Wang, B.; Luo, X. A cost-effective serpentine micromixer utilizing ellipse curve. *Anal. Chim. Acta* **2021**, *1155*, No. 338355.
(28) Ho, J.-Y.; Huang, M. H. Synthesis of Submicrometer-Sized Cu_2O Crystals with Morphological Evolution from Cubic to Hexapod Structures and Their Comparative Photocatalytic Activity. *J. Phys. Chem. C* **2009**, *113*, 14159−14164.